Topological Derivative: A Tool for Image Processing

I.Larrabide[a], R.A.Feijóo[a], A.A.Novotny[a] and E.A.Taroco[a]

[a] *LNCC - Laboratório Nacional de Computação Científica*
Rua Getúlio Vargas 333 - Petrópolis - RJ - Brazil
email: {nacho,feij,novotny,etam}@lncc.br

Abstract

The increasing complexity in several fields of science and technology has motivated the use of techniques originally conceived in other areas of applications. An illustrative example of this is given by the Topological Derivative which quantifies the sensitivity of a problem when the domain under consideration is perturbed by changing its topology. This concept, initially conceived to deal with topology optimization problems, has also been successfully applied to inverse problems and material properties characterization. Our aim in this paper is to present an other field of application for the topological derivative: *image processing*. An appropriate functional and a variational problem are associated to the cost endowed to an specific image processing application. Thus, the corresponding topological derivative can be used as an indicator function that leads, through a minimization process, to the processed image. We focus our attention on two image processing application. In the first, the topological derivative is used in image restoration i.e. to restore an image that was somehow degraded (acquisition process, transmission, storage, etc.). Moreover, a novel fully discrete algorithm based on the topological derivative concept is presented. In the second application, we use the topological derivative to derive a "continuous" and a fully discrete novel image segmentation algorithm, i.e. for objects identification in an image. Finally and in order to show the performance of these algorithms, several numerical examples are also presented in this work.

Key words: Topological derivative, image restoration, image segmentation.

1 Introduction

As a consequence of the technological advance a variety of instruments and tools have been introduced in medicine. For instance, we can refer to medical imaging devices. More specifically, techniques like Computed Tomography

(CT), Magnetic Resonance Imaging (MRI), Single Photon Emission Tomography (SPECT), Positron Emission Tomography (PET) and Ultrasound (US) among others, have provided useful information (anatomical and functional) to specialists, no matter which is the area of interest (practical medicine, research, etc.). Therefore, the demand for tools to manipulate medical images has grown considerably since the appearance of these technologies. Also different issues have appeared in this field, and to recall some of them we can mention volume data visualization, image restoration, image segmentation, image registration, pattern recognition, etc.

The inherent complexity of this area has motivated interdisciplinary research and the use of techniques actually born in other areas into medical imaging, as is the case of image processing. In this work, we focus our attention in the Topological Derivative as a tool for image processing, specifically in image restoration and segmentation. As it is known, the topological derivative allows us to quantify the sensitivity of a problem when the domain under consideration is perturbed by changing its topology, for example by the introduction of an arbitrary shaped hole, an inclusion or a source term. Early work on this subject can be found in papers by Masmoudi, Sokolowsky and their co-workers (Masmoudi, 1987; Sokolowski and Żochowski, 1999). This derivative has been originally conceived as a tool to solve topology optimization problems. Nevertheless, this concept is wider and has shown interesting results when applied in inverse problems. See also Novotny (2003); Amstutz (2003); Céa *et al.* (2000); Eschenauer *et al.* (1994); Novotny *et al.* (2003); Masmoudi (2002) for applications of the topological derivative to the above equations topology optimization and inverse problems considering Navier, Laplace, Poisson, Helmoltz, Stokes and Navier-Stokes equations among others.

In this paper another field of application for the topological derivative namely image restoration and image segmentation is studied. In particular, the topological derivative has proven to be a powerful tool in this field of research (Auroux *et al.*, 2006; Belaid *et al.*, 2007; Hintermüler, 2005). We can also mention the work of He and Osher (2006), where a connection is made between level set and the topological derivative. More specifically, appropriated functionals and variational formulations associated to the cost endowed to image restoration and segmentation are proposed. The corresponding topological derivatives can be used as an indicator function that allow us to obtain, through a minimization process, the processed image. Following this approach, novel algorithms for image restoration and segmentation are proposed.

This article is organized as follows. In Section 2 the concept of topological derivative is introduced. The context of image restoration using the topological derivative is analyzed and a fully discrete algorithm that removes noise preserving details (edges) is proposed in Section 3. Furthermore several numerical applications are also presented in this section showing the effectiveness

of this new algorithm for image restoration. In Section 4, the image segmentation problem is tackled defining an appropriate functional and calculating its topological derivative. As shown in this section, "continuous" and fully discrete novel algorithms are also presented and used in segmenting several images with excellent performance.

2 The Topological Derivative

As mentioned above, the topological derivative (D_T) allows us to quantify the sensitivity of a problem when the domain under consideration is perturbed, for example by the introduction of an arbitrary shaped hole, an inclusion or a source term at an arbitrary point.

Then, let Ω be a bounded open set in $\mathbb{R}^N$ ($N = 2, 3$) and ω be a fixed bounded domain containing the origin. Let also $\mathcal{J}(u) = \mathcal{J}(u(\Omega))$ be the cost functional to be minimized and $u(\Omega)$ the solution of a variational problem defined over the domain Ω. For a small parameter $\epsilon \geq 0$, let $\Omega_\epsilon = \Omega - \overline{\omega}_\epsilon$ be the perturbed domain defined by inserting a small hole at point $\widehat{x} \in \Omega$ given by $\omega_\epsilon = \widehat{x} + \epsilon\, \omega$. Let also u_ϵ be the corresponding solution of the same variational problem but now defined over the perturbed domain Ω_ϵ.

For small values of ϵ the topological asymptotic expansion for $\mathcal{J}_\epsilon(u_\epsilon)$ reads

$$\mathcal{J}_\epsilon(u_\epsilon) = \mathcal{J}(u) + f(\epsilon) D_T(\widehat{x}) + o(f(\epsilon))\,, \tag{1}$$

where $f(\epsilon)$ is a known positive function going to zero with ϵ and $D_T(\widehat{x})$ is the topological derivative at point $\widehat{x}$. Since f is positive, by introducing a perturbation at any point $\widehat{x}$ where D_T is negative the cost function $\mathcal{J}$ will be decreased. Then, D_T can be taken as an indicator function defining the best places where the perturbations could be introduced in order to reduce the value of the cost function. As will be shown in the next sections, this information can be used to develop fast algorithms for image restoration and segmentation.

Furthermore, dividing Eq. (1) by $f(\epsilon)$ and after taking the limit $\epsilon \to 0$ we obtain

$$D_T(\widehat{x}) = \lim_{\epsilon \to 0} \frac{\mathcal{J}_\epsilon(u_\epsilon) - \mathcal{J}(u)}{f(\epsilon)}\,. \tag{2}$$

The numerator of the right hand side of the above expression is associated with the total variation of the cost function. This information will be used to derive a fully discrete algorithm for image restoration and segmentation.

3 Image Restoration via Topological Derivative

For visual analysis, clarity of details and object visibility are important features in medical images, but when the interest is to use more advanced image processing procedures like segmentation, a high signal-to-noise (SNR) is mandatory to reduce errors as much as possible.

Over the years different techniques have been studied to improve the SNR of a degraded image. These methods can be classified as those affecting acquisition time or pixel size (time averaging over pixels for repeated acquisitions, scanning with larger image elements), and methods not affecting these parameters (for example, improvement of the acquisition hardware and postprocessing the image data after acquisition, that is image processing techniques). The former techniques have the advantage of not affecting the acquisition process (Jain, 1989; Gonzalez and Woods, 2001). To this end different approaches have been proposed over the years. In particular, we can mention techniques based on the framework of variational approaches and energy minimization (Aubert and Kornprobst, 2002). The following energy was considered by these authors

$$\mathcal{J}(u) = \frac{1}{2}\int_{\Omega}(v-u)^2 d\Omega + \lambda \int_{\Omega} \phi(|\nabla u|)\, d\Omega. \tag{3}$$

In the above expression the first term measures the misfit between the (degraded) image data v and the restored image u and the second term is associated to the smoothing process. The parameter λ is used to control the weight given to each term. Moreover, the Euler equation for this functional is given by

$$-\lambda \,\mathrm{div}\left\{\frac{\phi'(|\nabla u|)}{|\nabla u|}\nabla u\right\} + u = v \tag{4}$$

together with homogeneous Newmann boundary condition on $\partial\Omega$. The authors also impose several restrictions over ϕ in order to ensure satisfactory noise reduction, as well as existence and uniqueness of the solution u which minimizes the functional in Eq. (3). Another approach for image restoration is based on nonlinear diffusion methods. In this case the evolution of the (restored) image $u = u(\mathbf{x}, t)$ is processed by a nonlinear anisotropic diffusion governed by a partial differential equation (PDE)

$$\frac{\partial u}{\partial t} = div\,(\mathbf{k}(|\nabla u|)\nabla u) \tag{5}$$

with initial condition $u_0 = v$ and where $\mathbf{k}(|\nabla u|)$ is a tensor field called diffusivity and is designed to steer the direction of the diffusion process. When $\mathbf{k}(|\nabla u|)$ is reduced to a constant k_0 the linear isotropic diffusion method is obtained. In order to improve the outcome of linear isotropic diffusion filtering, specially edge preservation, in Perona and Malik (1990) is introduced a

monotonically decreasing function $\phi(|\nabla u|)$ instead of the constant k_0 such that the diffusion flux is reduced over edges. Despite the fact that a number of different alternatives for function ϕ can be found in the literature, this approach is still limited due to the isotropic nature of the diffusion equation. In fact only the intensity of the diffusion flux is controlled preserving noise along edges. This highly undesirable property of the nonlinear isotropic diffusion method is partly reduced when a nonlinear anisotropic diffusivity tensor is introduced (see Frangakis and Hegerl (2001)). In that case, the diffusivity tensor $\mathbf{k}(|\nabla u|)$ is constructed from the eigenvectors and corresponding eigenvalues of the tensor $\mathbf{J} = (\nabla u \otimes \nabla u)$ and also satisfying that $\mathbf{k}(x) \to 0$ as $x \to \infty$. These conditions provoques denoising along edges and reduction of the diffusion in the presence of large gradients, for example, across boundaries. However, and since the diffusion across edges is not completely avoided, heuristic stop criteria must be introduced during the evolution in time otherwise details of the image may not be preserved. On the other hand and as will be shown in this paper, the methods based on the topological derivative also introduce anisotropic diffusion tensors with components taking a value k_0 in the direction diffusion is allowed (homogeneous regions of the image) and null otherwise (i.e., in the ortogonal direction of boundaries inside the image).

3.1 D_T image restoration - Continuum approach

An image restoration algorithm based on the topological derivative was proposed by Masmoudi and his collaborators in (Belaid *et al.*, 2005, 2007; Auroux *et al.*, 2006). The cost functional associated to the edge detection adopted by these authors is given by

$$\mathcal{J}(u) = \int_\Omega \nabla u \cdot \nabla u \, d\Omega \tag{6}$$

where $u \in H^1(\Omega)$ is the solution of the following variational equation

$$\int_\Omega (k_0 \nabla u \cdot \nabla \eta + u\,\eta)\, d\Omega = \int_\Omega v\,\eta \, d\Omega \;\forall \eta \in H^1(\Omega) \tag{7}$$

and v is the noisy image data. At any point $\mathbf{x} \in \Omega$, the topological derivative of the cost functional (Eq. (6)) when the domain perturbation is characterized by a straight crack with unit normal vector $\mathbf{n}$ orthogonal to the crack direction is obtained by these authors and is given by

$$D_T(\mathbf{x}, \mathbf{n}) = \mathbb{M}\mathbf{n} \cdot \mathbf{n} = -\pi \left(\nabla u \otimes_s \nabla p + \nabla u \otimes \nabla u\right) \mathbf{n} \cdot \mathbf{n} \tag{8}$$

where $p \in H^1(\Omega)$ is the solution of the *adjoint equation*

$$\int_\Omega (k_0 \nabla p \cdot \nabla \eta + p\,\eta)\, d\Omega = \int_\Omega \frac{\partial \mathcal{J}(u)}{\partial u}\, \eta \, d\Omega \;\forall \eta \in H^1(\Omega)\,. \tag{9}$$

Moreover, the orientation $\mathbf{n}$ of the crack at each point $\mathbf{x} \in \Omega$ is taken such that produces the minimum value for $D_T(\mathbf{x}, \mathbf{n})$. This is attained when $\mathbf{n}$ coincides with the eigenvector associated to the lowest eigenvalue, λ_{min}, of the symmetric tensor $\mathbb{M}$. Using this information the authors propose that the restored image $\overline{u} \in H^1(\Omega)$ is the solution of the variational problem (isotropic/anisotropic diffusion)

$$\int_\Omega (\mathbf{k}\nabla\overline{u} \cdot \nabla\eta + \overline{u}\,\eta)\, d\Omega = \int_\Omega v\,\eta\, d\Omega \;\forall \eta \in H^1(\Omega) \tag{10}$$

where the diffusivity tensor $\mathbf{k}(\mathbf{x})$ is adopted as

- Isotropic diffusion based on D_T:
  - $\mathbf{k}(\mathbf{x}) = \varepsilon\mathbf{I}$ if $D_T \leq \alpha D_{T,MIN}$;
  - $\mathbf{k}(\mathbf{x}) = k_0\mathbf{I}$ otherwise.
- Anisotropic diffusion based on D_T:
  - $\mathbf{k}(\mathbf{x}) = \varepsilon(\mathbf{n} \otimes \mathbf{n}) + k_0(\mathbf{t} \otimes \mathbf{t})$ if $D_T \leq \alpha D_{T,MIN}$;
  - $\mathbf{k}(\mathbf{x}) = k_0\mathbf{I}$ otherwise.

Then, to find the restored image $\overline{u}$ we must compute the solution of 3 systems of equations corresponding to the scalar fields u, p and $\overline{u}$.

At this point one question arises: is it possible to use the information given by the topological derivative in order to derive a fully discrete algorithm for image restoration without loss of quality when compared to the continuous approach?. The answer is affirmative and will be presented in the next section.

3.2 A fully discrete D_T based approach

Typically, medical images as CT or MRI, are three dimensional data sets. For the sake of simplicity we consider only one slice of the whole image volume [1], extending this idea to 3D is straightforward. The 2D image is characterized by a matrix of pixels, with an intensity associated to each one of them. More specifically, let us consider a two dimensional image v given by a set of $M \times N$ pixels s. At each pixel s the intensity of image v will be denoted v^s. Then, any medical image belongs to the space $\mathcal{U}^d$

$$\mathcal{U}^d := \{v; v^s = \text{constant in } \omega^s, s = 1 \cdots M \times N\}\ , \tag{11}$$

with $\Omega = \cup_s \overline{\omega^s}$, being ω^s the domain of pixel s. The set n^s of neighbors of a pixel s was defined as the 4 pixels [2] (see Fig. 1(a)) sharing a side with s.

[1] A 3D medical image is composed of a stack of 2D images.
[2] That is **w**est, **e**ast, **n**orth and **s**outh of pixel s.

The functional adopted for this fully discrete approach is taken as

$$\mathcal{J}^d(u_t^s) \;=\; \sum_s \sum_{p\in n^s} k^{s,p}\widehat{\Delta}u_t^{s,p}\cdot\widehat{\Delta}u_t^{s,p}\,, \tag{12}$$

which could be interpreted as a discrete approximation of the square of the energy norm of the field u. In the above expression the term $k^{s,p}$ is the diffusion coefficient of pixel s with neighbor p, $n^s=\{w,e,n,s\}$ stands for the neighbors of pixel s and $\widehat{\Delta}u_t^{s,p}$ is defined as

$$\widehat{\Delta}u_t^{s,p} = u_t^p - u_t^s\,. \tag{13}$$

In this case, u_t^s is not the solution of a variational problem, but is explicitly computed using the following expression

$$u_t^s(\mathbf{k}^s) \;=\; u_{t-1}^s + \lambda\sum_{p\in n^s} k^{s,p}\widehat{\Delta}u_{t-1}^{s,p} \tag{14}$$

where subindex $t\geq 1$ represents the iteration number, being $u_0^s = v^s$ the intensity of the original image at pixel s, $\mathbf{k}^s=\{k^{s,w},k^{s,e},k^{s,n},k^{s,s}\}$ denotes the set of diffusion coefficients associated to pixel s, $\lambda=\Delta t$ is the artificial time step size and with the notation $u_t^s(\mathbf{k}^s)$ we want to emphasize that u_t^s is an explicit function of the diffusion coefficients associated to pixel s. Finally, Eq. (14) can be seen as a finite difference approximation for Eq. (5).

3.3 Topological Derivative Computation

In the continuum approach, the introduction of a null (or very small) diffusion coefficient was interpreted as the creation of a hole or a crack. This will also be the case for the discrete approach. The fact that $k^{s,p}=0$ for pixel s with neighbor p is interpreted as introducing a crack along the edge they share (no diffusion occurs across this edge). Then, we want to find the best configuration for $\mathbf{k}^s$ that most preserve image details and remove noise when we compute u_t^s. As in this case u_t^s is an explicit function of the set $\mathbf{k}^s$, we are able to compute the **exact** *total variation* of the cost functional for a given perturbation in $k^{s,p}$. Moreover, let us denote by $\mathbf{k}_\epsilon^s$ the perturbed configuration on the diffusivity coefficients considered at pixel s then, the value of the cost functional when this perturbation is introduced is given by

$$\mathcal{J}^d(u_t^s(\mathbf{k}_\epsilon^s)) = \mathcal{J}^d(u_t^s(\mathbf{k}^s)) + D_T(s,\mathbf{k}_\epsilon^s) \tag{15}$$

where $D_T(s,\mathbf{k}_\epsilon^s)$ represents the *total variation* of the functional due to the perturbation on the diffusivity coefficients at pixel s characterized by the set $\mathbf{k}_\epsilon^s$. As in the continuum approach, by introducing a perturbation at pixel s where D_T is negative the cost functional $\mathcal{J}^d$ will be decreased. Then, using this

information we are able to select the best pixels for which this perturbation could be introduced.

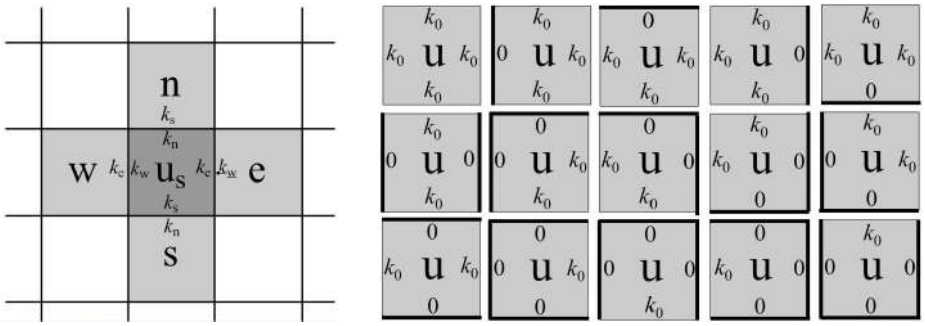

(a) Pixel s neighborhood and diffusion coefficient $\mathbf{k}^s$.

(b) Neighborhood cases.

Fig. 1. Pixel neighborhood considered.

To this end, we assume $k^{s,p} \in \{0, k_0\}$. Then, the set of all possible configurations for $\mathbf{k}^s$ can be defined as

$$\mathcal{C}(s) := \{\mathbf{k}^s = (k^{s,w}, k^{s,e}, k^{s,n}, k^{s,s}); k^{s,p} \in \{0, k_0\}, p = \{\text{w,e,n,s}\}\} \tag{16}$$

It is easy to notice that 16 different combinations are possible for $\mathbf{k}^s$ (the possibilities are $k^{s,p} = 0$ or $k^{s,p} = k_0$, for each neighbor, so $2^4 = 16$ cases are possible). The case $k^{s,w} = k^{s,e} = k^{s,n} = k^{s,s} = 0$ is discarded because, for this case, the cost function assumes the value 0 (and the original image is not changed). The remaining 15 combinations are

- do not apply diffusion with one neighbor,
- do not apply diffusion with two neighbors that share a vertex,
- do not apply diffusion with three neighbors,
- apply diffusion in x-direction,
- apply diffusion in y-direction,
- apply diffusion in all the directions (isotropic diffusion).

The last combination corresponds to isotropic diffusion and is defined by $\mathbf{k}^s_{iso} = \{k_0, k_0, k_0, k_0\}$. Since, the non perturbed configuration corresponds to the isotropic case we will denote by $\mathcal{C}_\sigma$ the subset of $\mathcal{C}$ containing the remaining $N_c = 14$ cases (Fig. 1(b)).

In order to compute the value of the D_T for a specific pixel, we need to introduce a perturbation. This is done by changing at a particular pixel s the set $\mathbf{k}^s_{iso}$ by $\mathbf{k}^s_\epsilon \in \mathcal{C}_\sigma$. Hence, the cost function $\mathcal{J}^d_\epsilon({}_\epsilon u^s_t)$ takes the form

$$\mathcal{J}^d_\epsilon({}_\epsilon u^s_t) \;=\; \mathcal{J}^d(u^s_t) - \sum_{p \in n^s} k^{s,p} \widehat{\Delta} u^{s,p}_t \cdot \widehat{\Delta} u^{s,p}_t + \sum_{p \in n^s} k^{s,p}_\epsilon \widehat{\Delta}\, {}_\epsilon u^{s,p}_t \cdot \widehat{\Delta}\, {}_\epsilon u^{s,p}_t \,, \tag{17}$$

for ${}_\epsilon u_t^s = u_t^s(\mathbf{k}_\epsilon^s)$ and $u_t^s = u_t^s(\mathbf{k}_{iso}^s)$ calculated using Eq. (14) and $\widehat{\Delta}\,{}_\epsilon u_t^{s,p} = u_t^p -_\epsilon u_t^s$.

Then, from Eqs. (15) and (17) the total variation of the cost function $\mathcal{J}^d$ due to the perturbation $\mathbf{k}_\epsilon^s$ can be written as

$$D_T(s, \mathbf{k}_\epsilon^s) \;=\; \sum_{p \in n^s} k_\epsilon^{s,p} \widehat{\Delta}\,{}_\epsilon u_t^{s,p} \cdot \widehat{\Delta}\,{}_\epsilon u_t^{s,p} - \sum_{p \in n^s} k^{s,p} \widehat{\Delta} u_t^{s,p} \cdot \widehat{\Delta} u_t^{s,p}. \qquad (18)$$

As in the continuum approach, the perturbation $\mathbf{k}_\epsilon^s$ (orientation of the crack at pixel s) is taken such that minimizes the value of $D_T(s, \mathbf{k}_\epsilon^s)$. Using this information we propose the following fully discrete image restoration algorithm based on the topological derivative (Algorithm 1).

Algorithm 1 Image restoration based on fully discrete version of the topological derivative

Require: A 2D image $v \in \mathcal{U}$ and the parameter α
Ensure: The restored image $\overline{u}^s \in \mathcal{U}$
  set $u_0^s = v^s$, t=1, Stop = FALSE
  $\mathbf{k}^s = \mathbf{k}_{iso}^s$, $s = 1..M \times N$
  while Stop = FALSE **do**
    for every pixel s **do**
      for every $\mathbf{k}_\epsilon^s \in \mathcal{C}_\sigma$ **do**
        compute $D_T(s, \mathbf{k}_\epsilon^s)$ following Eq. (18)
      end for
    end for
    set $D_T(s) = \min_{\epsilon^*}\{D_T(s, \mathbf{k}_\epsilon^s), \mathbf{k}_\epsilon^s \in \mathcal{C}_\sigma\}$
    for every pixel $s \in \mathcal{M}_\alpha$ **do**
      set $\mathbf{k}^s = \mathbf{k}_{\epsilon^*}^s$ the diffusivity coefficients associated to $D_T(s)$
    end for
    compute $u_t^s(\mathbf{k}^s)$ using Eq. (14).
    if $|\mathcal{J}_\epsilon^d({}_\epsilon u_t^s) - \mathcal{J}_\epsilon^d({}_\epsilon u_{t-1}^s)| > tol$ **then**
      $t = t + 1$
    else
      $\overline{u}^s = u_t^s, s = 1, \cdots, M \times N$, Stop = TRUE
    end if
  end while

The set $\mathcal{M}_\alpha$ is defined as

$$\mathcal{M}_\alpha := \{\, D_T(s) : D_T(s) < 0 \text{ and } D_T(s) \text{ is in the } \alpha\% \text{ most negative values of the } D_T\}. \qquad (19)$$

As in the continuum approach, in the above algorithm the α parameter allows

us to control the values of the topological derivative that will produce changes in $\mathbf{k}^s$. In the next section we present some results obtained using this technique.

3.4 Results

In order to show the performance of the proposed technique, in Figure 2 is presented the Lena image (size 256 × 256 pixels, polluted with $\sigma = 25$ White Gaussian Noise) processed with the nonlinear isotropic diffusion technique (Perona and Malik, 1990), the continuous D_T image restoration technique and the fully discrete version proposed in this work. In this case the following two alternatives for the function $\mathbf{k}(|\nabla u|)$ (nonlinear isotropic diffusion coefficient) where adopted

- Perona and Malik function (1990):

$$\mathbf{k}(x) \;=\; \frac{1}{1+\frac{x^2}{\sigma^2}} \tag{20}$$

- Tukey error norm function (Black *et. al.* (1998)):

$$\mathbf{k}(x) = \begin{cases} \frac{1}{2}\left(1-\frac{x^2}{\sigma^2}\right)^2 & |x| < \sigma \\ 0 & otherwise. \end{cases} \tag{21}$$

As can be seen, the results for the proposed method (D_T Discrete) are similar to the results for the other methods. Moreover, using the proposed fully discrete algorithm two different images were also processed. The first of these images (which will be referred as Case 1) is a phantom image with 200 × 204 pixels and composed of a series of elipses of sizes and shapes similar to the structures that could be found in a real medical image (see Kak and Roberts (1986) for more details about this image). Five different regions are present in this image: bg, intensity = 0; r_1, intensity = 70; r_2, intensity = 120; r_3, intensity = 170; r_4, intensity = 210. The non polluted image is presented in Fig. 3(b). This image was polluted using additive White Gaussian Noise (WGN) with different standard deviations σ ($\sigma = 18$ for Fig.3(c) and $\sigma = 25$ for Fig.3(d)).

These images were processed using different values for parameter α and the results are presented in Fig. 4. The first and second row correspond to the WGN $\sigma = 18$ and $\sigma = 25$ respectively. The columns correspond to the different values of parameter α (respectively and from left to right: 0.05, 0.10 and 0.15).

As we dispose of the original image, we are able to compute the error after the restoration process. To measure the quality of the results we use different

(a) Original Lena Image (b) Polluted Lena Image (c) D_T Continuous

(d) D_T Discrete (e) Perona and Malik (f) Tukey function

Fig. 2. Results for Lena Image.

error measures. Let v_0 be the original unpolluted image and $\overline{u}$ be the restored image, then

- Mean Square Error(MSE):

$$\text{MSE}(v_0, \overline{u}) = \frac{\sum_s (v_0^s - \overline{u}^s)^2}{(N \times M)} \tag{22}$$

- Peak Signal-to-Noise Ratio (PSNR):

$$\text{PSNR}(v_0, \overline{u}) = 10 * \log_{10} \left(\frac{max(\overline{u}^s)^2}{\text{MSE}(v_0, \overline{u})} \right) \tag{23}$$

- Signal-to-Noise Ratio (SNR):

$$\text{SNR}(v_0, \overline{u}) = 10 * \log_{10} \left(\frac{\frac{1}{N \times M} \sum_s (\overline{u}^s)^2}{\text{MSE}(v_0, \overline{u})} \right) \tag{24}$$

Also, we are able to compute the mean $\mu(e)$ and standard deviation $\sigma(e)$ of the error $e(s)$, being:

$$e(s) = v_0^s - \overline{u}^s, \tag{25}$$

$$\mu(e) = \frac{\sum_s e(s)}{(N \times M)}, \tag{26}$$

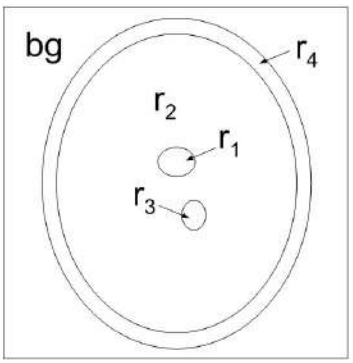

(a) Phantom image regions.

(b) Phantom image.

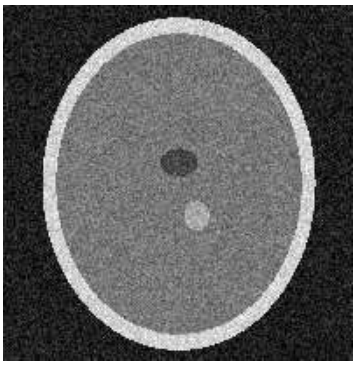

(c) Phantom image with $\sigma = 18$ WGN.

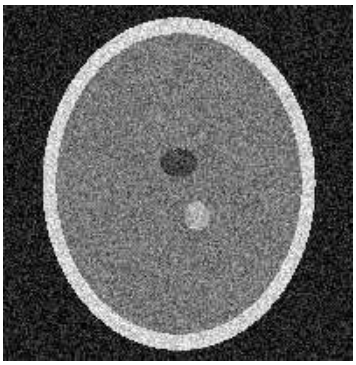

(d) Phantom image with $\sigma = 25$ WGN.

Fig. 3. Synthetic image - Case 1.

	PSNR	SNR	$\mu(e)$	$\sigma(e)$
WGN with $\sigma = 18$	23.156610	61.855321	-0.250686	17.728266
Result for $\alpha = 0.05$	34.160666	72.859376	0.227721	4.989477
Result for $\alpha = 0.10$	34.030855	72.729566	0.257525	5.063332
Result for $\alpha = 0.15$	33.016007	71.714718	0.201765	5.694655
WGN with $\sigma = 25$	20.334903	59.033613	-0.908284	24.518690
Result for $\alpha = 0.05$	31.595765	70.294476	-0.378824	6.699753
Result for $\alpha = 0.10$	31.075751	69.774462	-0.401863	7.113128
Result for $\alpha = 0.15$	30.068495	68.767206	-0.407647	7.990077

Table 1
Comparison table for Case 1.

$$\sigma(e) = \sqrt{\frac{\sum_s [\mu(e) - e(s)]^2}{(N \times M)}}. \tag{27}$$

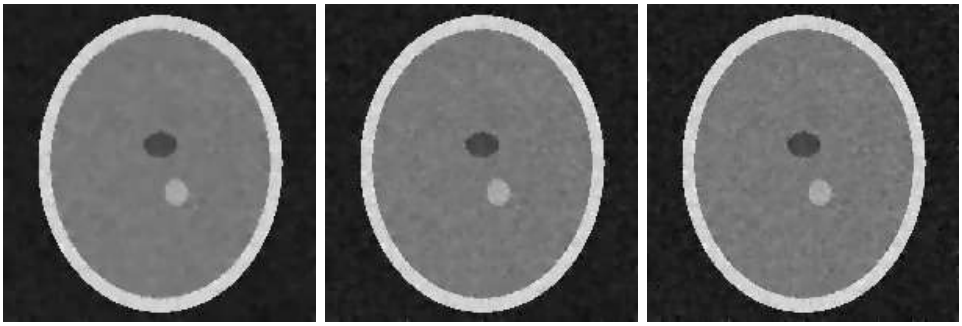

(a) $\sigma = 18$, $\alpha = 0.05$. (b) $\sigma = 18$, $\alpha = 0.10$. (c) $\sigma = 18$, $\alpha = 0.15$.

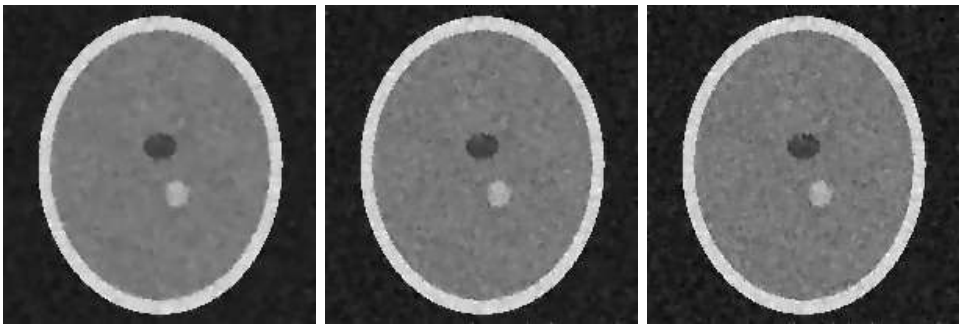

(d) $\sigma = 25$, $\alpha = 0.05$. (e) $\sigma = 25$, $\alpha = 0.10$. (f) $\sigma = 25$, $\alpha = 0.15$.

Fig. 4. Results for synthetic image - Case 1.

From the results presented in Table 1, we can observe that this method actually removes noise from the polluted image. When we analyze the statistical indicators, we observe that the mean of the error was reduced and the standard deviation σ was improved in $\approx 70\%$ in all cases.

As a second example we present another synthetic image with 256×256 pixels, in this case we also try to reproduce a medical image but with more complicated structures. Also the different structures present a smaller difference in their intensities. In this case 4 different regions are present: bg, intensity = 30; r_1, intensity = 50; r_2, intensity = 100; r_3, intensity = 150 (Fig. 5). As in the former case, this image was also polluted with different levels of WGN ($\sigma = 18$ for Fig.5(c) and $\sigma = 25$ for Fig.5(d)).

Following the same steps as in the first case, these images were processed using the proposed algorithm. Again, the same values for parameter α were tested. In Fig. 6 are presented the restored images for $\sigma = 18$ (first row) and $\sigma = 25$ (second row). In the columns are presented the images obtained for the different values of the parameter α (0.05, 0.10 and 0.15 from left to right respectively).

Again, the error was analyzed statistically and the results are presented in Table 2. In particular the statistical indicators point out an interesting improvement: the mean error remains close to 0 and the standard deviation σ

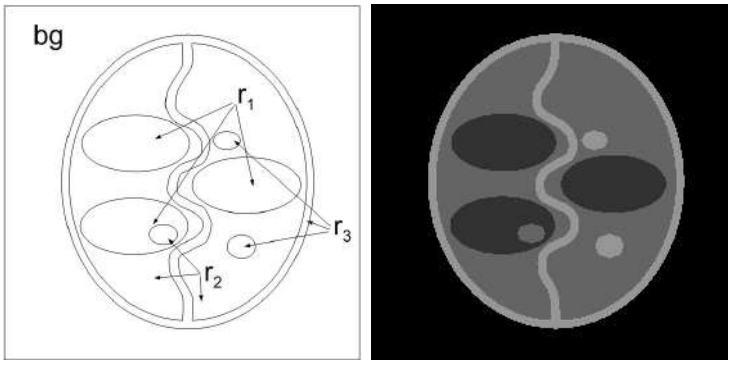

(a) Synthetic image regions. (b) Synthetic image.

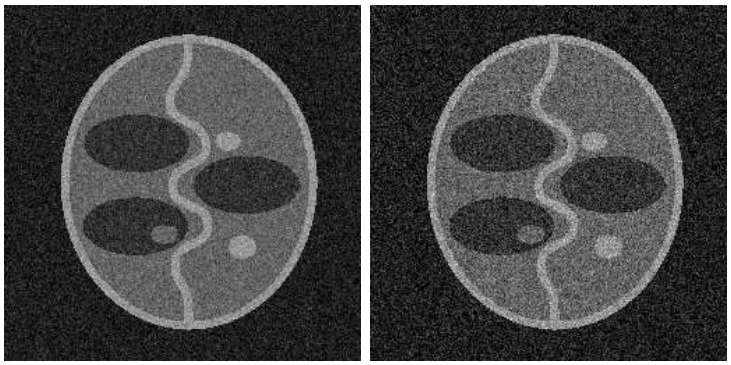

(c) Synthetic image with $\sigma = 18$ WGN. (d) Synthetic image with $\sigma = 25$ WGN.

Fig. 5. Synthetic image - Case 2.

	PSNR	SNR	$\mu(e)$	$\sigma(e)$
WGN with $\sigma = 18$	23.211969	60.561232	-0.168213	17.616593
Result for $\alpha = 0.05$	33.723066	71.072329	0.330505	5.242344
Result for $\alpha = 0.10$	33.064043	70.413307	0.327698	5.657319
Result for $\alpha = 0.15$	32.427279	69.776542	0.363342	6.087008
WGN with $\sigma = 25$	20.473755	57.823018	-0.940674	24.128072
Result for $\alpha = 0.05$	31.515300	68.864563	-0.431549	6.759146
Result for $\alpha = 0.10$	30.561596	67.910859	-0.396591	7.548520
Result for $\alpha = 0.15$	29.791046	67.140309	-0.364975	8.252082

Table 2
Comparison table for Case 2.

was improved in $\approx 65\%$.

As mentioned above, the topological derivative is used in an optimization process where we are interested in finding the optimal distribution for the diffusivity coefficients such that, in the presence of noise, will preserve image

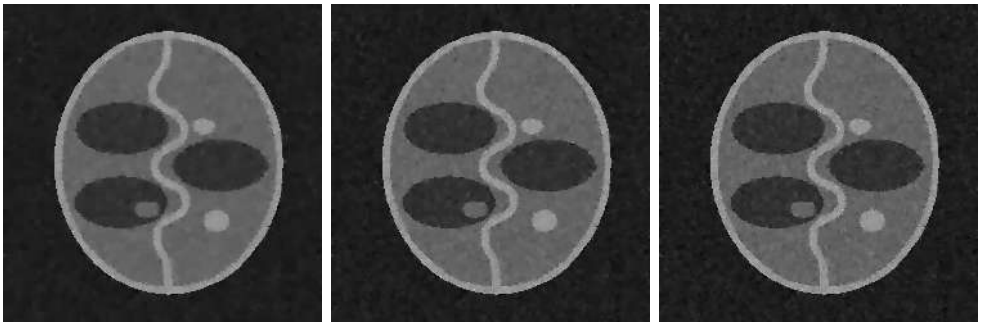

(a) $\sigma = 18$, $\alpha = 0.05$. (b) $\sigma = 18$, $\alpha = 0.10$. (c) $\sigma = 18$, $\alpha = 0.15$.

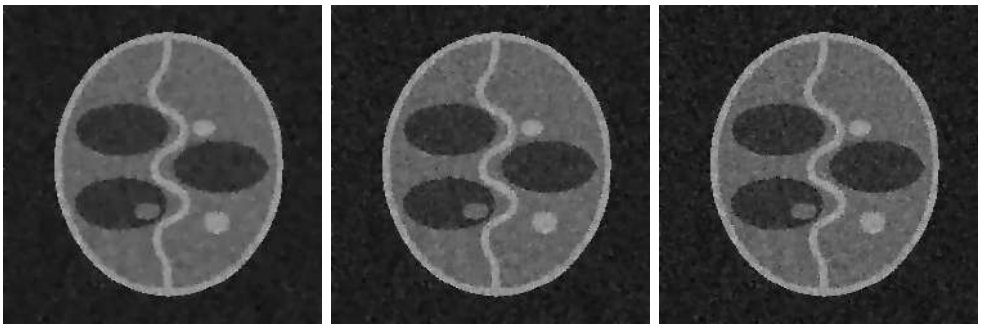

(d) $\sigma = 25$, $\alpha = 0.05$. (e) $\sigma = 25$, $\alpha = 0.10$. (f) $\sigma = 25$, $\alpha = 0.15$.

Fig. 6. Results for synthetic image - Case 2.

details eliminating noise. This process is stopped when the cost functional stabilizes and its variation in two consecutive iterations is smaller than a certain tolerance (denoted by *tol*). Fig. 7 presents the evolution of the cost functional as a function of iterations. As the number of iterations increase, the cost functional value stabilizes. This behavior also indicates that the restored image is stable with the number of iterations and no further degradation occurs as usually happens when nonlinear isotropic/anisotropic diffusion algorithms are used.

4 Image Segmentation via Topological Derivative

Medical imaging data provides information otherwise unavailable for clinical specialists to analise. Quantitative information such as organ size and shape can be extracted from these images in order to support different activities, as surgical planning, disease diagnosis and monitoring among others. The first step in this process is to identify the different tissues and anatomical structures present in the image. This process, called segmentation, subdivides an image into its constituent regions or objects and must be accurate and repeatable in order to be clinically useful. On the other hand, the level to which the subdivision is done depends on the particular application.

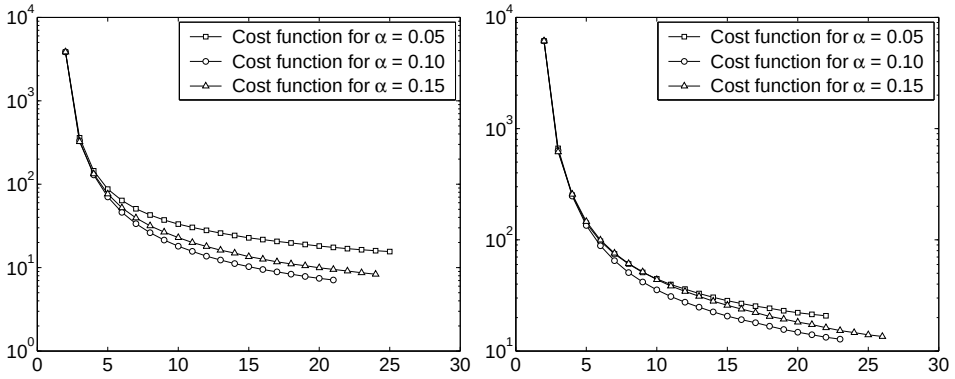

(a) Cost function for Case 1 and $\sigma = 18$.

(b) Cost function for Case 1 and $\sigma = 25$.

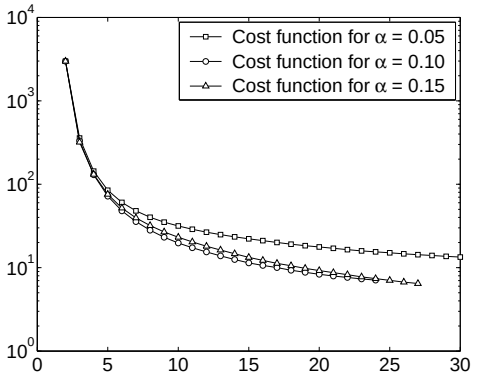

(c) Cost function for Case 2 and $\sigma = 18$.

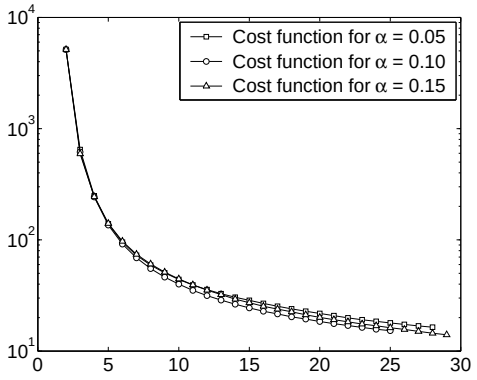

(d) Cost function for Case 2 and $\sigma = 25$.

Fig. 7. Cost function for the restoration problem (cost function value vs. iteration number).

Classical image segmentation techniques are based on two basic pixel characteristics: discontinuities and similarities. Many of this classical techniques (e.g., multiple thresholds, region growing, morphologic filtering and others (Jain, 1989; Gonzalez and Woods, 2001)) have been applied to try to solve this problem with variable outcomes (Suri *et al.*, 2001; Hohne *et al.*, 1990). Such techniques tend to be unreliable when segmenting a structure that is surrounded by others with similar image intensity (e.g., low-contrast structures).

More sophisticated techniques, like Level Sets, use powerful numerical computations for tracking the evolution of moving surface fronts. These techniques are based on computing linear/nonlinear hyperbolic equation solutions for the appropriate equations of motion. An initial approximation of the solution (seed) evolves until it gets the limits of the region of interest. In this case user interaction is needed to introduce one or more seeds for the algorithm to evolve from (Sethian, 1999; Malladi and Sethian, 1997). Although this approach brings good results, the computational cost may become too high. A wide variety of works present the Active Contour (also called Snakes)

technique as the most robust for medical image segmentation (Xu *et al.*, 2000, 1999; Li *et al.*, 1995; Boscolo *et al.*, 2002). With this technique good results are obtained, in particular for brain MRI segmentations. In this case input data must be pre-processed to extract spurious structures before the segmentation algorithm is started.

By means of Markov Random fields, in Held *et al.* (1997) and Zhang *et al.* (2001) fully automatic 3D-segmentation techniques especially designed for brain MRI images are described. These techniques capture three main spatial features of MRI images: non-parametric distribution of tissue intensities, neighborhood correlations and signal inhomogeneities. Once these fields are calculated (using suitable probabilistic models), an iterative optimization algorithm (Iterated Conditional Modes, Simulated Annealing, Expectation-Maximization, etc.) is used to recalculate them until convergence is achieved. Again, the limitation of this technique is its excessive computational cost.

In the next section we propose a novel image segmentation method based on the topological derivative. To this end an appropriate functional associated to the cost of a specific segmentation is proposed and the corresponding topological derivative is calculated in order to use it in a segmentation algorithm called D_T segmentation continuum approach. As was done in image restoration, in this section we also develop a discrete version of this method. Finally, several image segmentations with different levels of noise are presented and compared to classical methods in order to show the performance and capabilities of these two new methods (for a more exhaustive comparison see Larrabide *et al.* (2006)).

4.1 D_T image segmentation - Continuum approach

In this work the following cost functional is adopted (Larrabide *et al.*, 2006)

$$\mathcal{J}(\varphi) = \frac{1}{2}\int_\Omega \mathbf{k}\nabla\varphi\cdot\nabla\varphi\, d\Omega \; + \frac{1}{2}\int_\Omega (\varphi - (v-u))^2\, d\Omega, \tag{28}$$

where the diffusivity tensor $\mathbf{k}$ could be adopted as $\mathbf{k} = k_0\mathbf{I}$ (isotropic and homogeneous tensor) or, tensor $\mathbf{k}$ could be taken equal to the one obtained using the restoration algorithms proposed in Section 3. Also in the above expression $v \in \mathcal{V}$ is the image data, $u \in \mathcal{U}$ is the segmented image and $\mathcal{V}$ and $\mathcal{U}$ are defined respectively by

$$\mathcal{V}{:=}\{w \in L^2(\Omega) :\ w^s \text{ constant at } s\text{-pixel/voxel level}\}, \tag{29}$$

$$\mathcal{U}{:=}\{u \in \mathcal{V} : u(x) \in \mathcal{C}, \forall x \in \Omega\}. \tag{30}$$

The set $\mathcal{C}$ characterizes the number of classes (Nc) for which the original image v will be segmented, and is defined as

$$\mathcal{C}:=\{c_i \in \mathbb{R} : i = 1...Nc\} \ , \tag{31}$$

where c_i is the intensity associated to the i_{th} class. Moreover, φ is the solution of the following variational problem: Find $\varphi \in H^1(\Omega)$ such that

$$\begin{cases} a(\varphi, \eta) = l(\eta) \ \ \forall \eta \in H^1(\Omega), \\ \varphi \in H^1(\Omega) \end{cases}$$

with $a(\cdot,\cdot) : H^1(\Omega) \times H^1(\Omega) \to \mathbb{R}$ and $l(\cdot) : H^1(\Omega) \to \mathbb{R}$

$$a(\varphi, \eta) := \int_\Omega \mathbf{k}\nabla\varphi \cdot \nabla\eta \ d\Omega + \int_\Omega \varphi\eta \ d\Omega, \tag{32}$$

and

$$l(\eta) := \beta \int_\Omega (v - u)\eta \ d\Omega. \tag{33}$$

To identify a class different alternatives can be used. The values defined for the classes will depend on the specific application of the segmentation. Therefore, we will obtain different results according to the criteria adopted to define the set of classes $\mathcal{C}$ (for instance, mean intensity inside a region). Other image information can be used to determine this values. In the case of CT the brighter intensities represent bone and darker areas represent soft tissues as inner organs or muscles. This *a priori* information can be used to determine classes values.

Associated to φ is defined the function φ_ϵ that is the solution of the same variational formulation but now defined on the perturbed problem. The perturbation is introduced by changing the segmented image u with a new one u_T which is identical to u at every point of the domain Ω except in the small region B_ϵ centered at point $\widehat{x} \in \Omega$. In B_ϵ, u_T assumes one of the values $c_i \in \mathcal{C}$. Then, the perturbed cost functional becomes

$$\mathcal{J}_\epsilon(\varphi_\epsilon) = \frac{1}{2}\int_\Omega (\varphi_\epsilon - (v - u_T))^2 \ d\Omega + \frac{1}{2}\int_\Omega \mathbf{k}\nabla\varphi_\epsilon \cdot \nabla\varphi_\epsilon \ d\Omega, \tag{34}$$

where the field φ_ϵ is the solution of the perturbed variational problem: Find $\varphi_\epsilon \in H^1(\Omega)$ such that

$$\begin{cases} a(\varphi_\epsilon, \eta) = l_\epsilon(\eta) \ \ \forall \eta \in H^1(\Omega), \\ \varphi_\epsilon \in H^1(\Omega) \end{cases}$$

with $a(\cdot,\cdot) : H^1(\Omega) \times H^1(\Omega) \to \mathbb{R}$ defined as before and $l_\epsilon(\cdot) : H^1(\Omega) \to \mathbb{R}$

defined as

$$l_\epsilon(\eta) = \beta \int_\Omega (v - u_T)\eta \, d\Omega. \tag{35}$$

The associated adjoint problem is given by: Find $p_\epsilon \in H^1(\Omega)$ such that

$$\begin{cases} a(p_\epsilon, \eta) = -\left\langle \frac{\partial}{\partial \varphi_\epsilon} \mathcal{J}_\epsilon(\varphi_\epsilon), \eta \right\rangle \quad \forall \eta \in H^1(\Omega), \\ p_\epsilon \in H^1(\Omega) \end{cases}$$

Is easy to verify that

$$p_\epsilon = \frac{(1-\beta)}{\beta} \varphi_\epsilon. \tag{36}$$

Using topological shape sensitivity analysis, the topological derivative for this problem is computed (Larrabide *et al.*, 2006). In this case, the $D_T(\widehat{x})$ is given by

$$\begin{aligned} D_T(\widehat{x}) = & \frac{1}{2}(c_i - u)\left[\left(\varphi\left(\widehat{x}\right) - (v-u)\right) + \left(\varphi(\widehat{x}) - (v - c_i)\right) + \right. \\ & \left. + 2\left(1-\beta\right)\varphi\left(\widehat{x}\right)\right] \quad \forall \widehat{x} \in \Omega. \end{aligned} \tag{37}$$

and the topological asymptotic expansion reads

$$\mathcal{J}(\varphi_\epsilon) = \mathcal{J}(\varphi) + f(\epsilon) D_T(\widehat{x}) + o(f(\epsilon)). \tag{38}$$

Then, introducing a perturbation at points where D_T is negative the cost functional will be decreased. Using this information, the Algorithm 2 (continuum approach) for image segmentation is proposed.

Algorithm 2 Image segmentation based on the topological derivative D_T

Require: An input image $v \in L^2(\Omega)$, the set of classes $\mathcal{C}(\Omega)$, an initial guess $u_0 \in \mathcal{U}$ and the parameters β and **k**

Ensure: The segmented image $u^* \in L^2(\Omega)$

```
while ∃ D_T < 0 do
    solve the variational problem (32) to obtain φ_n,
    compute D_T at each point x̂ ∈ Ω
    if min_i{D_T((x̂)), i = 1, ..., N_c} < 0 then
        u(x̂) = c_i
    end if
    make n = n + 1 and u_{n+1} = u,
end while
u* = u_{n+1}
```

4.2 A fully discrete D_T based approach

In this work is proposed an alternative segmentation algorithm based on a simplification of the former idea. As we will show, for the discrete case it is not necessary to compute the field φ to obtain the topological derivative.

In fact, taking $\beta = 0$ in Eq.(32) we obtain the trivial solution $\varphi \equiv 0$ for any segmented image $u \in \mathcal{U}$. In this case also the cost functional $\mathcal{J}(\varphi)$ reduces to a functional $\mathcal{J}(\cdot) : \mathcal{U} \to \mathbb{R}$ and given by

$$\mathcal{J}(u) = \int_{\Omega} (v - u)^2 \, d\Omega \tag{39}$$

With this in mind, let us consider a two-dimensional image [3] characterized by a set of $M \times N$ pixels s with $\overline{\Omega} = \cup_s \overline{\omega^s}$. For each pixel s we denote by v^s and by u^{*s} the intensity of the function $v \in \mathcal{V}^d$ and of the segmented image $u^* \in \mathcal{U}^d$ respectively and where the sets $\mathcal{V}^d \subset \mathcal{V}$ and $\mathcal{U}^d \subset \mathcal{U}$ are defined as

$$\mathcal{V}^d := \{v;\ v^s \text{ constant in } \omega^s; s = 1...M \times N\} \ , \tag{40}$$

$$\mathcal{U}^d := \{u;\ u^s \in \mathcal{C}; s = 1...M \times N\} \ . \tag{41}$$

Furthermore, the following cost functional is adopted

$$\mathcal{F}^d(u^s) = \theta \mathcal{J}^d(u^s) + (1 - \theta)\mathcal{B}^d(u^s) \ , \quad \text{with} \quad \theta \in (0, 1] \subset \mathbb{R} \ , \tag{42}$$

where the first term of the cost function $\mathcal{F}^d(u^s)$, denoted by $\mathcal{J}^d(u^s)$, is associated to the *distance* between the input image pixels intensities v^s and the segmented image pixels intensities u^s. This term can be interpreted as the discrete version of the functional given by Eq.(39). The second term $\mathcal{B}^d(u^s)$ can be seen as a regularization functional that measures (and penalizes) the interface (boundary) length between different regions. These terms respectively take the form

$$\mathcal{J}^d(u^s) \ = \ \sum_s (v^s - u^s)^2 \quad \text{and} \quad \mathcal{B}^d(u^s) \ = \ \frac{1}{4n} \sum_s \sum_{p=\{w,e,n,s\}} \chi(u^s, u^p) \ , \tag{43}$$

where $n = 2$ ($n = 3$) for 2-dimensional (3-dimensional) images and $\chi(u^s, u^p)$ is a characteristic function of the boundary that the pixel s shares with the neighbor pixel p and is defined as taking the value 1 (one) when $u^s \neq u^p$ and 0 otherwise. The θ parameter controls the contribution of each term ($\mathcal{J}^d(u^s)$ and $\mathcal{B}^d(u^s)$) to the cost function $\mathcal{F}^d$. When we are interested in classifying pixels of the image in homogeneous regions, the size of the interfaces between

[3] Extending this idea to 3D is straightforward.

both regions will produce a higher value of the cost function. This is done by setting $\theta < 1$.

4.3 Topological Derivative Computation

In order to compute the topological derivative, we need to perturb the cost function at a given pixel s. This is done by changing the class of pixel s from u^s to c_i. In this way we obtain the perturbed cost functional $\mathcal{F}^d(u_T^s)$ given by

$$\mathcal{F}^d(u_T^s) \;=\; \theta\mathcal{J}^d(u_T^s) + (1-\theta)\mathcal{B}^d(u_T^s)\;, \tag{44}$$

where $\mathcal{J}^d(u_T^s)$ and $\mathcal{B}^d(u_T^s)$ can be written as

$$\begin{aligned}
\mathcal{J}^d(u_T^s) &= \mathcal{J}^d(u^s) - (v^s - u^s)^2 + (v^s - c_i)^2,\\
\mathcal{B}^d(u_T^s) &= \mathcal{B}^d(u^s) - \frac{1}{4n}\sum_{p=\{w,e,n,s\}} (\chi(u^s, u^p) - \chi(c_i, u^p))\\
&\qquad \text{for } i = 1\cdots Nc.
\end{aligned} \tag{45}$$

where u_T^s is equal to u^s everywhere but in the pixel s it assumes the value c_i.

Then, the total variation of the functional $\mathcal{F}^d$ will be denoted by D_T and is given by the difference $\mathcal{J}^d(u_T^s) - \mathcal{J}^d(u^s)$, that is

$$\begin{aligned}
D_T(u_T^s) &= \theta\left[(v^s - u_T^s)^2 - (v^s - u^s)^2\right] + (1-\theta)\frac{1}{4n}\sum_{p=\{w,e,n,s\}} [\chi(u_T^s, u^p) - \chi(u^s, u^p)]\\
&\qquad \text{for } u_T^s = c_i, i = 1\cdots Nc.
\end{aligned} \tag{46}$$

Moreover, at each pixel s the perturbation u_T^s will be selected such that produces the minimum value for the total variation at that pixel.

4.4 An Image Segmentation Algorithm

Using the information given by the total variation, a fully discrete topological derivative segmentation algorithm for 2D images (Algorithm 3) is proposed in this work. The algorithm inputs are the 2D image $v \in \mathcal{V}^d$ to be segmented and a set of classes in witch image pixels will be classified. The algorithm output is $\bar{u}^* \in \mathcal{U}^d$. As mentioned before, the topological derivative can be used as a descent criterion in an optimization process. The sufficient local minimum condition is given by

$$D_T(u_T^s) \geq 0 \quad \forall\; s = 1, \ldots, N \times M \tag{47}$$

Algorithm 3 Image segmentation algorithm based on the Topological Derivative

Require: A 2D image $v \in \mathcal{V}^d$, the set of classes $\mathcal{C}$, $\theta \in (0, 1]$ and an initial guess $u_0 \in \mathcal{U}^d$
Ensure: The segmented image $\bar{u}^* \in \mathcal{U}^d$
  normalize the image and classes values to $[0, 1]$
  while $\exists\ T$ and s such that $D_T(u_T^s) < 0$ **do**
    for every pixel s **do**
      for every class $c_i \in \mathcal{C}$ **do**
        compute $D_T(u_T^s)$ following (Eq. 46)
      end for
      if $\min_{\bar{T}}\{D_T(u_T^s),\ \ T = 1, \ldots, N_c\} < 0$ **then**
        $u^s = c_{\bar{i}}$
      end if
    end for
  end while
  $\bar{u}^{*s} = u^s$, $s = 1 \ldots N \times M$

Depending on the case, the stop condition could be substituted by a criteria associated to the behavior of the cost functional, i.e., if in two consecutive iterations, the cost function decreased less than a certain given tolerance, the algorithm stops.

In some cases (e.g., strong noise), changing **all** the pixels whose topological derivative is negative, an oscillating behavior was observed. This problem was solved using the same technique shown in Algorithm 1. That is, only a percent of the pixels whose topological derivative is negative is taking in each step. This simple technique stabilizes the algorithm and produces a convergent result in all the cases.

4.5 Experimental Results

The quality of the corresponding segmented images was quantified using the following metrics (Alonso *et al.*, 2004; Zijdenbos *et al.*, 1994)

- **Tanimoto index:** This index is calculated as

$$I(A_1, A_2) = \frac{n(A_1 \cap A_2)}{n(A_1 \cup A_2)}\,. \tag{48}$$

- **Overlap index:** Is defined as (Zijdenbos *et al.*, 1994):

$$O(A_1, A_2) = 2 \cdot \frac{n(A_1 \cap A_2)}{n(A_1) + n(A_2)}\,. \tag{49}$$

- **Mass Center Deviation (MCD):** Is computed as the distance from the exact center of mass of a particular region and the corresponding region in the segmented image. This computation includes **all** the pixels in the segmented image that were classified in that region.
- **Distance between borders (DBB):** This index is given by

$$D(C_1, C_2) = \frac{\sum_{i=1}^{np1} d(x_1^i, C_2) + \sum_{i=1}^{np2} d(x_2^i, C_1)}{(np1 + np2)} \tag{50}$$

  where $d(x, C)$ means the distance (in pixels) of the point x to the curve C, C_1 and C_2 are the boundaries of the original and segmented region respectively, x_1^i and x_2^i denote arbitrary points on the boundaries C_1 and C_2, finally $np1$ and $np2$ are the number of points which characterize the respective boundaries.

The D_T methods (Continuous and Discrete) where compared to other well established segmentation methods (Bootstrap, Fuzzy C-Means and K-means) usually used to segment medical images. In Figure 8 are presented the comparisons for the mentioned methods and indexes. As can be seen, only K-means is able to keep up with the results of both D_T methods.

Furthermore, using the Case 1 and Case 2 images shown in Section 3 the behavior of the DT discrete segmentation method was analyzed for different alternatives in the noise roving process. The considered alternatives are: no processing (NPP), 3 iterations (ISPP3), 6 iterations (ISPP6) of isotropic smoothing (convolution with a 5×5 gaussian kernel), and finally the D_T Restoration method was used to remove noise (DTPP, with $\alpha = 0.05, 0.10, 0.15$). The values used to characterize the classes were exactly the intensities of the corresponding regions in the original synthetic image. For Case 1 the classes were bg, intensity = 30; c_1, intensity =70; c_2, intensity = 120; c_3, intensity = 170 and c_4, intensity = 210 (Fig. 3). The corresponding segmented images are presented in Fig. 9.

As before, the quality of the segmentation was analyzed using the indexes presented above. In particular, Table 3 presents the results of the D_T Discrete for Case 1 image with the same level of noise yet considered ($\sigma = 18$ and $\sigma = 25$). Moreover, Fig. 9 presents the segmented images. In all cases our method together with the DTPP noise removal has shown good results.

For Case 2 the classes were bg, intensity = 30; c_1, intensity = 50; c_2, intensity = 100 and c_3, intensity = 150. As in the case presented before, 6 different alternatives where studied (NPP, ISPP3, ISPP6 and DTPP, with $\alpha = 0.05, 0.10, 0.15$) and in Fig. 10 the obtained segmented images are presented. The quality of the segmentations using the mentioned indexes is presented in Table 4 and the obtained segmentations are shown in Fig. 10. Again, the D_T Discrete method

	Class	MCD	Overlap	Tanimoto	DBB
NPP, $\sigma = 18$	bg	0.063243	0.995661	0.994204	2.075105
	c_1	4.231997	0.896082	0.814241	1.132450
	c_2	0.044466	0.998734	0.998277	0.057111
	c_3	4.544380	0.916031	0.861244	0.050032
	c_4	0.233750	0.993105	0.990374	0.238770
ISPP3, $\sigma = 18$	bg	0.165457	0.879011	0.844935	2.063228
	c_1	9.761395	0.332429	0.200984	0.900806
	c_2	0.066079	0.927756	0.892451	0.715043
	c_3	19.784325	0.106437	0.056640	1.058168
	c_4	0.647279	0.000000	0.000000	1.834747
ISPP6, $\sigma = 18$	bg	0.196921	0.821802	0.775725	3.094668
	c_1	10.422243	0.200105	0.113623	1.296074
	c_2	0.055267	0.898263	0.851011	1.028865
	c_3	20.920997	0.056616	0.029343	1.484937
	c_4	7.043816	0.000000	0.000000	10.256423
DTPP, $\alpha = 0.05$, $\sigma = 18$	bg	0.039016	0.998967	0.998623	0.896736
	c_1	2.445294	0.840691	0.784946	0.455503
	c_2	0.028159	0.996661	0.994840	0.076508
	c_3	8.908987	0.701595	0.574627	0.066256
	c_4	0.088697	0.981293	0.975212	0.045464
DTPP $\alpha = 0.10$, $\sigma = 18$	bg	0.072224	0.998450	0.997934	1.306487
	c_1	4.348604	0.925532	0.867110	0.924401
	c_2	0.015530	0.996873	0.995693	0.333505
	c_3	5.870391	0.876847	0.798206	0.192099
	c_4	0.195792	0.993330	0.991051	0.071340
DTPP $\alpha = 0.15$, $\sigma = 18$	bg	0.125568	0.993891	0.988305	4.425880
	c_1	5.543596	0.000000	0.000000	0.633329
	c_2	0.067099	0.993930	0.991763	0.678158
	c_3	6.392879	0.794872	0.661922	0.525449
	c_4	0.226113	0.984548	0.979353	0.162338
NPP, $\sigma = 25$	bg	0.137028	0.980815	0.974099	7.192250
	c_1	10.198286	0.512255	0.360967	4.887185
	c_2	0.051609	0.980622	0.973561	1.723486
	c_3	15.840950	0.690763	0.540881	1.019918
	c_4	0.367261	0.977055	0.968236	0.910857
ISPP3, $\sigma = 25$	bg	0.190733	0.874346	0.839197	2.153920
	c_1	10.190951	0.327804	0.197442	0.941402
	c_2	0.085705	0.928545	0.893469	0.710956
	c_3	19.163325	0.109000	0.058037	1.040971
	c_4	0.954842	0.000000	0.000000	1.835030
ISPP6, $\sigma = 25$	bg	0.211291	0.814928	0.767575	3.210187
	c_1	10.874960	0.229804	0.131157	1.317803
	c_2	0.125370	0.904393	0.858668	0.980922
	c_3	19.937577	0.051317	0.026572	1.427957
	c_4	8.164308	0.000000	0.000000	7.443467
DTPP $\alpha = 0.05$, $\sigma = 25$	bg	0.093383	0.995172	0.993516	2.781506
	c_1	8.695588	0.692029	0.589506	1.667984
	c_2	0.119534	0.987511	0.982133	0.228436
	c_3	17.063908	0.459215	0.308943	0.145423
	c_4	0.191939	0.926130	0.903322	0.199796
DTPP $\alpha = 0.10$, $\sigma = 25$	bg	0.086234	0.994540	0.992600	3.307148
	c_1	7.928047	0.726968	0.609551	2.381302
	c_2	0.051243	0.988749	0.984102	1.003429
	c_3	13.530365	0.636183	0.486322	0.638370
	c_4	0.130446	0.965860	0.953611	0.143955
DTPP $\alpha = 0.15$, $\sigma = 25$	bg	0.099157	0.992988	0.990256	4.545317
	c_1	6.611247	0.644654	0.511222	3.158723
	c_2	0.056550	0.984811	0.979095	1.484264
	c_3	17.314316	0.615970	0.461538	0.928605
	c_4	0.321158	0.969213	0.958562	0.163003

Table 3
Comparison table for segmentation results - Case 1.

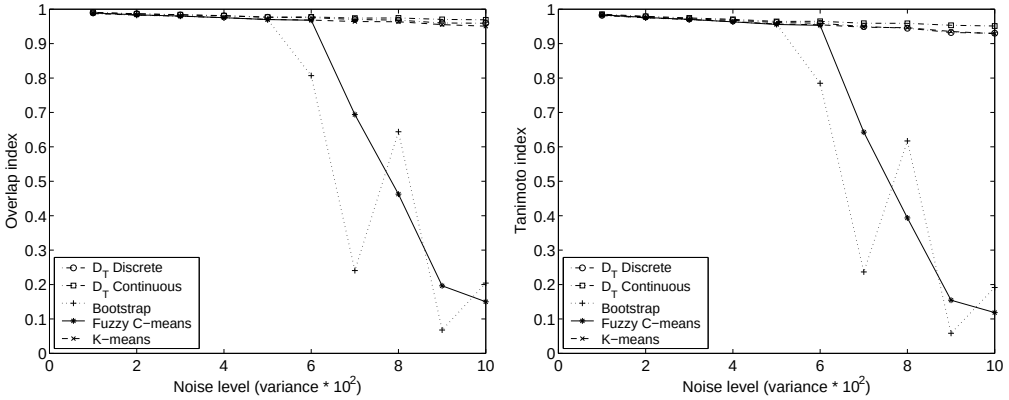

(a) Overlap index.

(b) Tanimoto index.

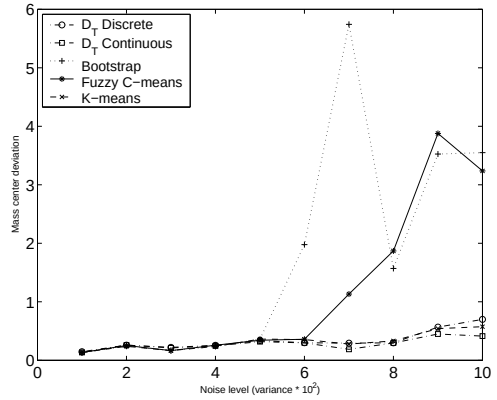

(c) Mass center deviation.

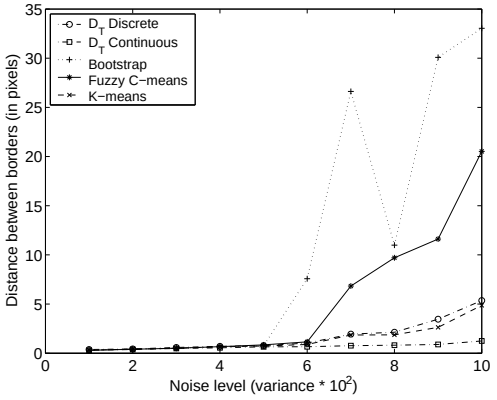

(d) Distance between borders.

Fig. 8. Curves for the indexes used to compare the methods. All plots are organized as index value for y coordinate and noise variance for x coordinate. The variances varies from 0.01 to 0.1 in 0.01 increments (for the image intensities normalized to the interval $[0, 1]$).

performs better when the TDPP preprocessing is adopted.

Finally and for Case 1, the behavior of the cost functional given by Eq. (42) as a function of iterations is presented in Fig. 11 (WGN with $\sigma = 18$ and $\sigma = 25$ in Fig. 11(a) and 11(b) respectively).

5 Conclusions

In this paper was presented a new area of application for the topological derivative: image processing, in particular to image restoration and segmentation. Four algorithms D_T *continuum approach* and D_T *fully discrete* for image restoration and image segmentation are proposed. These algorithms are based on computing the topological derivative for an appropriate cost functional and using this information to characterize the perturbation to be inserted. This

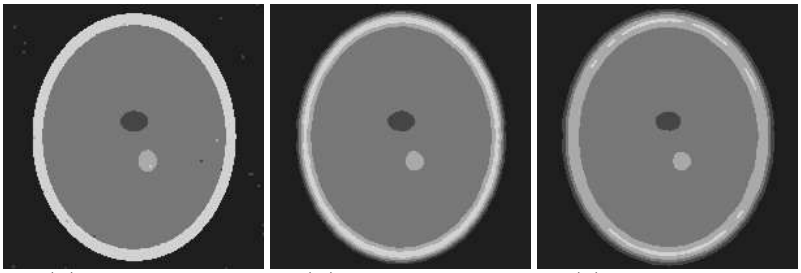

(a) $\sigma = 18$, NPP. (b) $\sigma = 18$, ISPP3. (c) $\sigma = 18$, ISPP6.

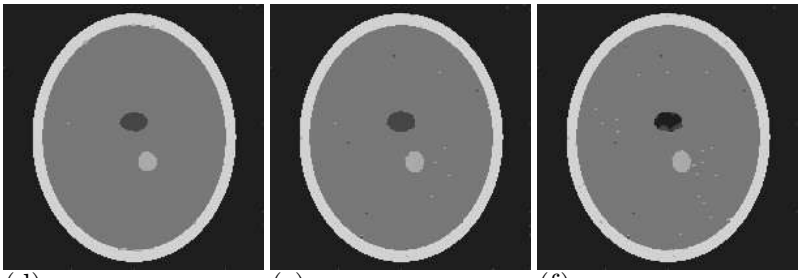

(d) $\sigma = 18$, DTPP with $\alpha = 0.05$. (e) $\sigma = 18$, DTPP with $\alpha = 0.10$. (f) $\sigma = 18$, DTPP with $\alpha = 0.15$.

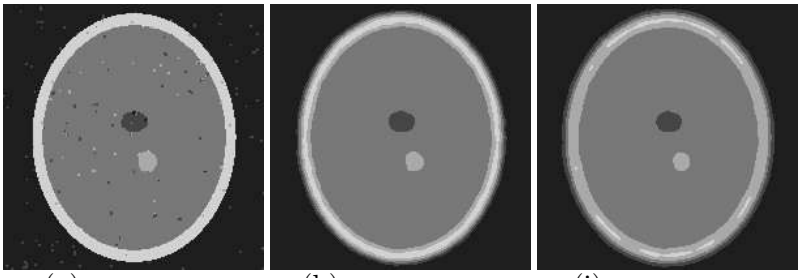

(g) $\sigma = 25$, NPP. (h) $\sigma = 25$, ISPP3. (i) $\sigma = 25$, ISPP6.

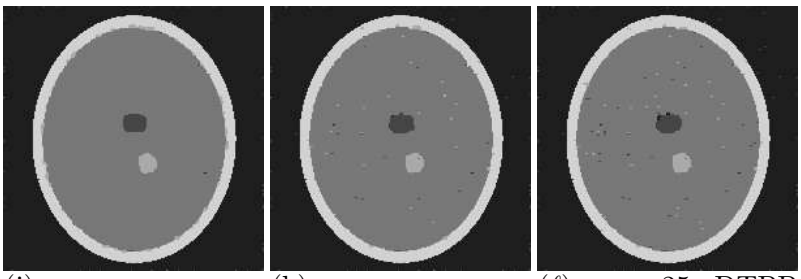

(j) $\sigma = 25$, DTPP with $\alpha = 0.05$. (k) $\sigma = 25$, DTPP with $\alpha = 0.10$. (ℓ) $\sigma = 25$, DTPP with $\alpha = 0.15$.

Fig. 9. Results for synthetic image - Case 1.

novel approach gives the appropriate diffusivity tensor at any point of the domain that can be used for noise elimination and gives the most appropriate pixel classification during the segmentation process.

The algorithms were tested with synthetic images degraded with different noise levels and compared with methods already used for these issues. In all cases the proposed algorithms are able to produce excellent results even for images degraded with strong noise where the others methods generally fails. Finally,

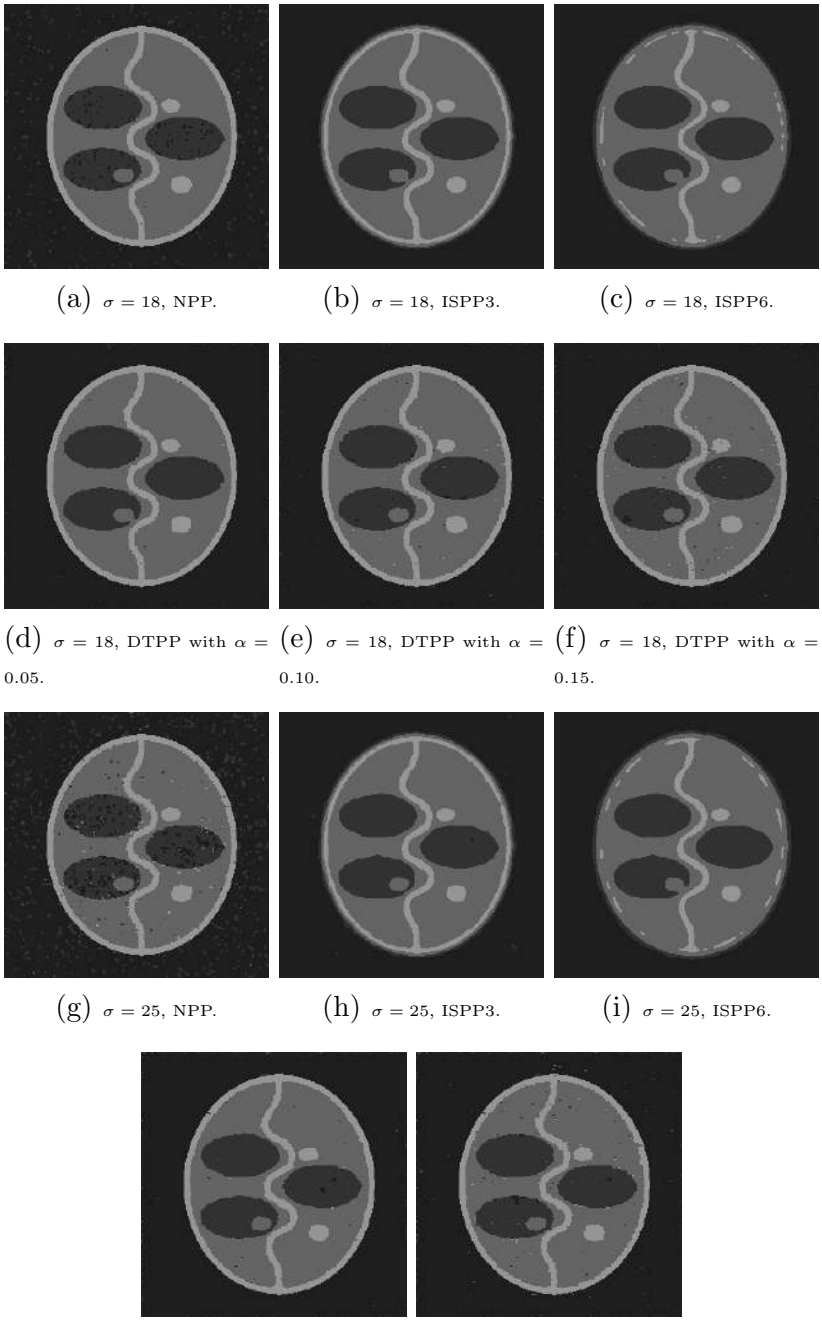

(a) $\sigma = 18$, NPP. (b) $\sigma = 18$, ISPP3. (c) $\sigma = 18$, ISPP6.

(d) $\sigma = 18$, DTPP with $\alpha = 0.05$. (e) $\sigma = 18$, DTPP with $\alpha = 0.10$. (f) $\sigma = 18$, DTPP with $\alpha = 0.15$.

(g) $\sigma = 25$, NPP. (h) $\sigma = 25$, ISPP3. (i) $\sigma = 25$, ISPP6.

(j) $\sigma = 25$, DTPP with $\alpha = 0.05$. (k) $\sigma = 25$, DTPP with $\alpha = 0.10$.

Fig. 10. Results for synthetic image - Case 2.

concerning the convergence issues for image processing algorithms based on topological derivative, we refer the reader to Belaid *et al.* (2005, 2007).

	Class	MCD	Overlap	Tanimoto	DBB
NPP, $\sigma = 18$	bg	0.498795	0.925491	0.898359	24.988116
	c_1	2.230574	0.782898	0.686635	11.357807
	c_2	0.070907	0.989726	0.984340	0.302543
	c_3	0.214670	0.977240	0.967281	0.079201
ISPP3, $\sigma = 18$	bg	0.447994	0.920598	0.896860	2.430799
	c_1	1.717762	0.895116	0.817590	0.763943
	c_2	0.396328	0.941890	0.894251	0.519422
	c_3	0.635437	0.560402	0.487152	0.714340
ISPP6, $\sigma = 18$	bg	0.596886	0.891943	0.860933	3.367975
	c_1	2.186333	0.856791	0.759035	0.987164
	c_2	0.698385	0.896412	0.815712	0.950743
	c_3	2.384734	0.000000	0.000000	3.709368
DTPP, $\alpha = 0.05$, $\sigma = 18$	bg	0.028543	0.990160	0.986687	13.555566
	c_1	0.204234	0.961343	0.937861	5.178683
	c_2	0.377372	0.980026	0.968986	0.306938
	c_3	1.234920	0.943759	0.920871	0.219132
DTPP $\alpha = 0.10$, $\sigma = 18$	bg	0.041923	0.987798	0.982859	16.180620
	c_1	0.148215	0.949456	0.921411	5.628081
	c_2	0.311331	0.976744	0.965784	0.526392
	c_3	0.851640	0.949262	0.924965	0.419549
DTPP $\alpha = 0.15$, $\sigma = 18$	bg	0.101573	0.983861	0.977126	18.301397
	c_1	0.707214	0.927620	0.889621	6.842766
	c_2	0.098943	0.973103	0.961079	0.853432
	c_3	0.172514	0.953219	0.929760	0.651386
NPP, $\sigma = 25$	bg	1.178724	0.847396	0.796283	26.726824
	c_1	4.960136	0.511747	0.395506	13.859100
	c_2	0.192516	0.946047	0.922430	2.105597
	c_3	0.530470	0.934613	0.898838	1.423971
ISPP3, $\sigma = 25$	bg	0.520017	0.914074	0.888571	4.122567
	c_1	1.884506	0.877452	0.791894	1.313068
	c_2	0.452387	0.931905	0.881464	0.558374
	c_3	1.036228	0.553777	0.478422	0.760443
ISPP6, $\sigma = 25$	bg	0.660702	0.882783	0.849587	3.672161
	c_1	2.187299	0.830688	0.725929	1.127844
	c_2	0.895636	0.891374	0.809281	0.997886
	c_3	4.484137	0.000000	0.000000	2.595335
DTPP $\alpha = 0.05$, $\sigma = 25$	bg	0.112122	0.986012	0.980894	15.565098
	c_1	0.561304	0.942178	0.909935	7.348805
	c_2	0.431706	0.963539	0.945628	1.085454
	c_3	1.242042	0.921996	0.887155	0.403577
DTPP $\alpha = 0.10$, $\sigma = 25$	bg	0.084423	0.982120	0.975029	18.493928
	c_1	0.675668	0.920735	0.879487	8.488288
	c_2	0.508348	0.949835	0.927024	1.770457
	c_3	1.148880	0.912646	0.872428	0.827229
DTPP $\alpha = 0.15$, $\sigma = 25$	bg	0.064728	0.976656	0.967037	21.434197
	c_1	0.475470	0.885048	0.831336	9.997039
	c_2	0.509805	0.934349	0.905783	2.551882
	c_3	1.186147	0.901604	0.854825	1.333364

Table 4
Comparison table for segmentation results - Case 2.

6 ACKNOWLEDGMENTS

This research was partly supported by the brazilian agencies CNPq/FAPERJ-PRONEX, under Grant E-26/171.199/2003. Ignacio Larrabide was partly supported by the brazilian agency CNPq (141336/2003-0). The support of these

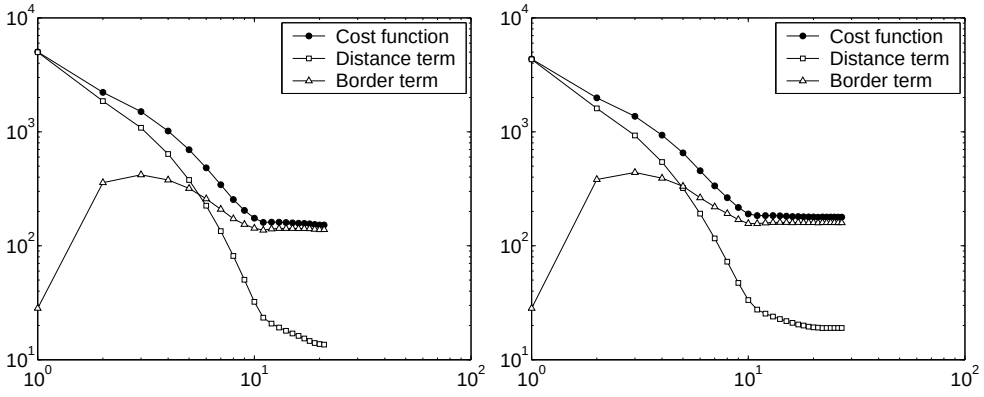

(a) (b)

Fig. 11. Cost function for Case 1 with $\sigma = 18$ and 25, with $\alpha = 0.05$ (cost function value vs. iteration number).

agencies is greatly appreciated.

References

Alonso, F., Algorri, M., and Flores-Mangas, F. (2004). Composite index for the quantitative evaluation of image segmentation results. In *Proceedings of the 26th Annual International Conference of the IEEE EMBS*, pages 1794–1797, San Francisco, CA, USA.

Amstutz, S. (2003). *Aspects théoriques et numériques en optimisation de forme topologique*. Phd thesis, Institut National des Sciences Appliquées de Toulouse, France.

Aubert, G. and Kornprobst, P. (2002). *Mathematical Problems in Image Processing*, volume 147 of *Applied Mathematical Sciences*. Springer-Verlag.

Auroux, D., Masmoudi, M., and Belaid, L. (2006). Image restoration and classification by topological asymptotic expansion. *Variational Formulations in Mechanics: Theory and Applications - CIMNE, Barcelona, Spain 2006 (In press)*.

Belaid, L. J., Jaoua, M., Masmoudi, M., and Siala, L. (2005). Image restoration and edge detections by topological asyptotic expansion. Masmoudi personal communication.

Belaid, L. J., Jaoua, M., Masmoudi, M., , and Siala, L. (2007). Application of the topological gradient to image restoration and edge detection. *To apper on Special Issue on "Shape and Topological Sensitivity Analysis: Theory and Application" of the Engineering Analysis with Boundary Element Journal*.

Boscolo, R., Brown, M., and McNitt-Gray, M. (2002). Medical image segmentation with knowledge-guided robust active contours. *Radiographics*, **22**(2), 437–448.

Céa, J., Garreau, S., Guillaume, P., and Masmoudi, M. (2000). The shape

and topological optimizations connection. *Computer Methods in Applied Mechanics and Engineering*, **188**(4), 713–726.

Eschenauer, H. A., Kobelev, V. V., and Schumacher, A. (1994). Bubble method for topology and shape optimization of structures. *Structural Optimization*, **8**, 42–51.

Frangakis, A. S. and Hegerl, R. (2001). Noise reduction in electron tomographic reconstructions using nonlinear anisotropic diffusion. *J. Struct. Biol.*, **1**(135), 239–250.

Gonzalez, C. R. and Woods, R. E. (2001). *Digital Image Processing - Second Edition*. Prentice Hall.

He, L. and Osher, S. (2006). Solving the chan-vese model by multiphase level set algorithm based on the topological derivative. Technical Report 56, UCLA - CAM.

Held, K., Kops, E. R., Krause, B. J., 3rd, W. M. W., Kikinis, R., and Muller-Gartner, H. W. (1997). Markov random field segmentation of brain mr images. *IEEE Trans. Med. Imaging*, **16**(6), 878–886.

Hintermüler, M. (2005). Fast level set based algorithms usind shape and topological sensitivity. *Control and Cybernetics*, **34**(1), 305–324.

Hohne, K. H., Fuchs, H., and Pizer, S. M. (1990). *3D imaging in medicine: algorithms, systems, applications*. Springer-Verlag, New York.

Jain, A. K. (1989). *Fundamentals of Digital Image Processing*. Prentice Hall.

Kak, A. C. and Roberts, B. (1986). *Handbook of Pattern Recognition and Image Processing*. T.Y.Young and K.S.Fu, Eds. NY - Academic Press.

Larrabide, I., Novotny, A. A., Feijóo, R. A., and Taroco, E. (2006). Topological derivative as a tool for image processing: Image segmentation. Technical report, LNCC - Laboratório Nacional de Computação Científica.

Li, H., Deklerck, R., DeCuyper, B., Hermanusa, A., Nyssen, E., and Cornelis, J. (1995). Object recognition in brain ct-scans: knowledge-based fusion of data from multiple feature extractors. *IEEE Trans. Med. Imaging*, **14**, 212–229.

Malladi, R. and Sethian, J. A. (1997). Level set methods for curvature flow, image enhancement, and shape recovery in medical images. In *Proc. of Conf. on Visualization and Mathematics*, pages 329–345, Germany. Springer-Verlag.

Masmoudi, M. (1987). *Outils pour la Conception Optimale de Formes*. Phd thesis, Nice University.

Masmoudi, M. (2002). The topological asymptotic. *Computational Methods for Control Applications, Ed. H.Kawarada and J.Périaux, International Series GAKUTO*.

Novotny, A., Feijóo, R., Taroco, E., and Padra, C. (2003). Topological sensitivity analysis. *Computer Methods in Applied Mechanics and Engineering*, **192**, 803–829.

Novotny, A. A. (2003). *Análise de Sensibilidade Topológica*. Phd thesis, Laboratorio Nacional de Computação Científica, Petrópolis - RJ - Brazil.

Perona, P. and Malik, J. (1990). Scale-space and edge detection using

anisotropic diffusion. *IEEE Trans. Pattern Anal. Machine Intell.*, **12**(7), 629–639.

Sethian, J. A. (1999). *Level Set Methods and Fast Marching Methods*. Cambridge University Press.

Sokolowski, J. and Żochowski, A. (1999). Topological derivatives for elliptic problems. *Inverse Problems*, **15**, 123–134.

Suri, J., Singh, S., and Setarehdan, K., editors (2001). *Advanced algorithmic approaches to medical image segmentation: state-of-the-art applications in cardiology, neurology, mammography and pathology*. Springer-Verlag.

Xu, C., Pham, D. L., Rettmann, M. E., Yu, D. N., and Prince, J. L. (1999). Reconstruction of the human cerebral cortex from magnetic resonance images. *IEEE Transactions on Medical Imaging*, **18**(6), 467–480.

Xu, C., Pham, D. L., and Prince, J. L. (2000). *Medical Image Segmentation Using Deformable Models*, pages 129–174. SPIE Handbook on Medical Imaging - Volume III: Medical Image Analysis.

Zhang, Y., Brady, M., and Smith, S. (2001). Segmentation of brain mr images through a hidden markov random field model and the expectation-maximization algorithm. *IEEE Transactions on Medical Imaging*, **20**(1), 45–57.

Zijdenbos, P., Dawant, B. M., Margolin, R. A., and Palmer, A. C. (1994). Morphometric analysis of white matter lesions in mr images: Method and validation. *IEEE Trans. Med. Imag.*, **13**(4), 716–724.